





Research paper

# Application of optical flow methods to aerated skimming flows above triangular and trapezoidal step cavities

GANGFU ZHANG , Postdoctoral Research Fellow, *School of Civil Engineering, The University of Queensland, Brisbane, Australia.*

Email: [gangfu.zhang@uqconnect.edu.au](mailto:gangfu.zhang@uqconnect.edu.au) (author for correspondence)

HUBERT CHANSON  (IAHR Member), Professor, *School of Civil Engineering, The University of Queensland, Brisbane, Australia.*

Email: [h.chanson@uq.edu.au](mailto:h.chanson@uq.edu.au)

## ABSTRACT

Stepped chutes are built to provide safe flood passage in dams. The steps are associated with strong turbulence generation, which allow air to be entrained from the free surface. The present work adopts a non-intrusive local optical flow technique to examine the effects of partial cavity blockage on the mean and turbulent properties in aerated skimming flows in two large-size stepped chute models. The partial cavity blockage was found to be associated with decreased mean velocities in the overflow. The step edge was identified as the most significant source of turbulent production. General increases in turbulence levels and large scale turbulent motions were identified for the partially blocked cavities, which could be linked to a reduction in mutual sheltering between adjacent roughness elements. It was implied that the cavity blockage might have some effects on the velocity gradient fluctuations.

*Keywords:* Macro roughness; multiphase flow; optical flow; physical modelling; stepped spillway; turbulence

## 1 Introduction

Stepped spillways are structures designed to facilitate the safe passage of flood waves in dams (Chanson, 2001). The steps trigger a turbulent boundary layer growth from the upstream end of the chute (Chanson, 1994; Wood, Ackers, & Loveless, 1983). At the intersection between the boundary layer outer edge and free surface, turbulent stresses exceed the combined effect of surface tension and buoyancy, thus leading to air-entrainment (Chanson, 1993, 2008; Ervine & Falvey, 1987; Rao & Rajaratnam, 1961). The aerated flow region is characterized by extremely complex air–water interactions and presents a significant measurement challenge to experimental physicists.

Stepped chute flows were traditionally investigated using intrusive techniques (e.g. phase-detection probe, optic fibre probe), which are generally of high accuracy but restricted to point measurements. More recently, image-based velocimetry has become more accessible because of the advancement in computational power and reduction in hardware cost. Amador, Sánchez-Juny, and Dolz (2006) characterized a non-aerated skimming flow using particle image velocimetry (PIV). In

later studies, a modified technique known as bubble image velocimetry (BIV) was applied to aerated skimming flows by Bung (2011) and Leandro, Bung, and Carvalho (2014) under ordinary lighting conditions. The BIV presents an intuitive solution, although limited by its discrete data nature (Chen & Katz, 2005; Corpetti, Heitz, Arroyo, Memin, & Santa Cruz, 2006). Alternatively, the apparent flow motion may be derived using differential techniques that take advantage of the continuous textural patterns typical of air–water flow images. Known as optical flow methods, these were successfully applied to aerated flows in the works of Bung and Valero (2016a, 2016b, 2016c) and validated by Zhang and Chanson (2018). Compared to BIV, optical flow methods, when properly calibrated, are capable of producing velocity data with better accuracy and at much higher resolutions (Liu, Merat, Makhmalbaf, Fajardo, & Merati, 2015).

A number of studies have proposed an analogy between flow over stepped chutes and those above transverse square bars (e.g. Chanson, Yasuda, & Ohtsu, 2002; Gonzalez & Chanson, 2008). The latter is typically classified as either a “d-type” or a “k-type”, depending on the roughness density (Djenidi, Elavasaran, & Antonia, 1999). Perry, Schofield, and Joubert

Received 7 July 2017; accepted 12 June 2018/Open for discussion until 29 February 2020.

(1969) suggested that d- and k-type roughness exhibit distinctive vortex shedding characteristics, which might further modulate the mean flow properties. Previous investigations of such interplay were primarily based on local measurement of interfaces (e.g. Felder & Chanson, 2011; Gonzalez & Chanson, 2004, 2008; Guenther, Felder, & Chanson, 2013; Takahashi, Gonzalez, & Chanson, 2006; Zhang & Chanson, 2016a), and the problem remains to be addressed in a global, non-intrusive manner.

The goal of the present investigation is to examine the effects of partial blockage of unmodified triangular cavities (i.e. trapezoidal cavities) by the application of a non-intrusive optical technique. Detailed flow visualizations were performed with an ultra-high-speed camera. The mean and turbulent apparent flow motions were analysed using the Farneback optical flow method. The present analysis aims to improve understandings of significant flow processes governed by the cavity geometry.

## 2 Experimental set-up

The present study was conducted under very calm inflow conditions in a large-size steep chute ( $\theta = 45^\circ$ ) at the University of Queensland (UQ). A smooth and stable discharge was delivered by three pumps driven by adjustable frequency AC motors. The chute inflow was controlled by an upstream broad-crested weir made of smooth, painted marine ply. The model discharge was obtained by integrating the velocity distributions above the upstream broad-crested weir (Zhang & Chanson, 2016b). Cavity effects on aerated skimming flows were tested in two large-size stepped spillway models, sketched in Fig. 1. The base model (I) consisted of 12 uniform triangular steps made of smooth marine ply, each measuring  $0.1 \times 0.1 \times 1.0$  m (height  $\times$  length  $\times$  width). The same model was used in Zhang and Chanson (2016b, 2018). The modified set-up (II) was configured with triangular blockages to the step corners with sides equalling 33% of the step height (Fig. 1).

Detailed air–water flow patterns for a dimensionless discharge  $d_c/h = 0.9$  were investigated with a Phantom<sup>®</sup> v2011 ultra-high-speed camera (Vision Research, USA), mounted at approximately 60 cm from the chute sidewall (Fig. 2). Images were recorded through a Nikkor 50 mm f/1.4 lens (Nikon, Japan) with a negligible degree of barrel distortion ( $\sim 1.3\%$ ). The camera was tilted  $45^\circ$  in the flow direction to achieve equal pixel densities ( $\text{px mm}^{-1}$ ) in both the streamwise and normal directions. The flow was illuminated by a  $4 \times 6$  high-intensity LED matrix fixed to steel mullions supporting the channel sidewall. The angle of the light was adjusted so that the illumination intensity was as visually uniform as possible. During all experiments, the frame rate and resolution were 22,607 fps and  $1,280 \times 800$  px, respectively. The exposure time was kept at approximately  $1 \mu\text{s}$  to ensure sharp images. It is acknowledged that the subjectivity of the visual method to verify the constancy of illumination might limit the accuracy of the present study.

## 3 Image processing

The mean flow deformations and turbulence quantities were derived from raw 8-bit image sequences using a local optical flow technique. A variety of optical flow techniques were adopted by previous studies of high-speed air–water flows (e.g. Bung & Valero, 2016a, 2016b, 2016c), and a further validation study was performed by Zhang and Chanson (2018). The optical flow is defined as the apparent motion field between two consecutive images, and its physical meaning depends on the projective nature of the corresponding moving objects in 3D camera space. Existing algorithms attempt to recover the optical flow from spatial and temporal derivatives, and may be classified into local (e.g. Farneback, 2003; Lucas & Kanade, 1981) and global (e.g. Horn & Schunck, 1981) methods. The present study adopts the Farneback (2003) method capable of estimating the global optical flow despite being a local technique. Farneback (2003) proposed that the intensity information in the

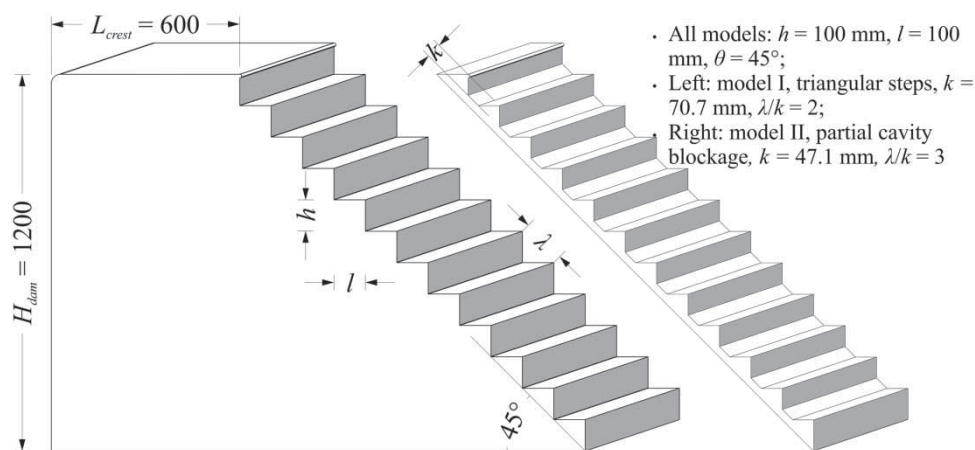


Figure 1 Definition sketch of stepped spillway models (units: mm). Left: base model (I) with uniform triangular steps. Right: modified model (II) with partially blocked step cavities

neighbourhood of a pixel might be modelled with a quadratic polynomial:

$$f_1(\mathbf{x}) \cong \mathbf{x}^T \mathbf{A}_1 \mathbf{x} + \mathbf{b}_1^T \mathbf{x} + c_1 \quad (1)$$

where  $x$  is the pixel coordinates in a local coordinate system,  $\mathbf{A}_1$  is a symmetric matrix,  $\mathbf{b}_1$  is a vector and  $c_1$  is a scalar. After a shift by  $\mathbf{d}$ , the displaced neighbourhood may be obtained by transforming the initial approximation:

$$\begin{aligned} f_2(\mathbf{x}) &= \mathbf{x}^T \mathbf{A}_2 \mathbf{x} + \mathbf{b}_2^T \mathbf{x} + c_2 \\ &= f_1(\mathbf{x} - \mathbf{d}) \\ &= \mathbf{x}^T \mathbf{A}_1 \mathbf{x} + (\mathbf{b}_1 - 2\mathbf{A}_1 \mathbf{d})^T \mathbf{x} + \mathbf{d}^T \mathbf{A}_1 \mathbf{d} - \mathbf{b}_1^T \mathbf{d} + c_1 \quad (2) \end{aligned}$$

and the displacement is then solved by equating the coefficients of  $\mathbf{x}$ :

$$\begin{aligned} \mathbf{b}_2 &= \mathbf{b}_1 - 2\mathbf{A}_1 \mathbf{d}, \\ \mathbf{d} &= -\frac{1}{2} \mathbf{A}_1^{-1} (\mathbf{b}_1 - \mathbf{b}_2) \quad (3) \end{aligned}$$

In practice, the displacement  $\mathbf{d}$  may be assumed slow-varying, and is solved for a neighbourhood of  $\mathbf{x}$ . Large displacements may be treated with a multi-resolution technique (i.e. image pyramid) (e.g. Adelson, Anderson, Bergen, Burt, & Ogden, 1984; Bung & Valero, 2016a; Burt & Adelson, 1983), in which  $\mathbf{d}$  obtained from successively subsampled images are used as *a priori* estimates of the true optical flow. Note that the accurate estimation of  $\mathbf{d}$  hinges on a negligible degree of luminance change for the region under consideration between two successive frames.

For the present study, optical flow computations were implemented in Python 2.7.9 with OpenCV 3.1.0. Note that optical flow estimations are not necessarily physical: compared to phase-detection probe data (obtained at approximately 2 mm from wall), a decrease in data quality (i.e. > 10% difference) was observed for void fractions greater than 50% (Zhang & Chanson, 2018). Nevertheless, the algorithm yields superior performance (i.e. five times faster as well as yielding a much denser velocity field) than a standard PIV according to the synthetic image benchmark by Bung and Valero (2017).

## 4 Results

### 4.1 Presentation

Ultra-high-speed videos were recorded in stepped chutes I and II for a skimming flow discharge  $d_c/h = 0.9$ . The air–water flow patterns between step edges 5 and 8 were examined. Each video was recorded for a duration of 1.472 s and subsampled at 4521 Hz (i.e. every fifth frame) prior to optical flow computations to improve efficiency. The corresponding physical resolutions of the videos ranged between 0.32 and 0.36 mm  $\text{px}^{-1}$  in both  $x$ - and  $y$ -directions.

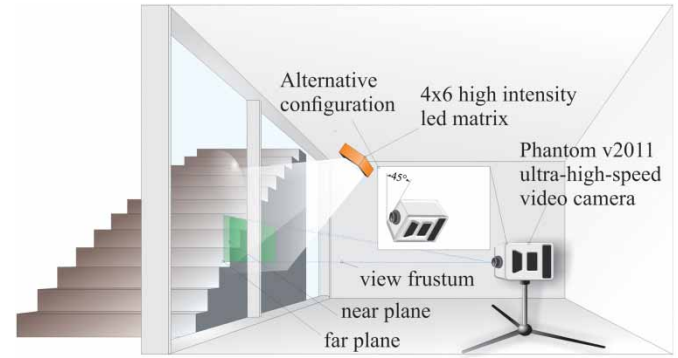


Figure 2 Ultra-high-speed video camera set-up

The Farneback algorithm (2003) was applied to consecutive pairs of raw images to extract the optical flow. This yielded Eulerian measurements of apparent motions at every pixel location within the camera frame. Polynomial expansions were calculated for a neighbourhood of 7 px, smoothed by a Gaussian window with a standard deviation of 1 px. The displacements were averaged over a window size of 15 px. Additional analyses were undertaken to determine the optical turbulence intensity, mean flow deformation, and relevant time/length scales. Note that the optical flow results do not guarantee a correspondence with physically meaningful flow features; instead, the non-intrusive approach provides further insight into the complex air–water flow structures and complements traditional measurement techniques such as intrusive phase-detection probes.

### 4.2 Mean optical flow fields

Figure 3 presents the dimensionless streamwise ( $U_o$ ) and normal ( $V_o$ ) optical flow distributions between step edges 5 and 8 in stepped chute models I (Fig. 3a–b) and II (Fig. 3c–d). In Fig. 3,  $x$  is the streamwise coordinate originating from step edge 1,  $y$  is the normal distance from the pseudo-bottom,  $x_i$  is the location of the inception point of free-surface aeration,  $L_{cav}$  is the distance between adjacent step edges ( $= 0.141$  m), and  $U_c (= (gd_c)^{0.5})$  is the critical flow velocity. The results for  $y/d_c > 0.6$ – $0.7$  were truncated since discontinuous flow features lead to unreliable optical flow estimates (Zhang & Chanson, 2018).

For both stepped chute models, the results showed an accelerating flow motion. The flow field consisted of a supercritical, coherent overflow, and a slow, recirculating cavity region, separated by the pseudo-bottom connecting the step edges. Strong flow detachment was observed at each step edge. In the mainstream, the streamwise optical flow was larger for the triangular cavities (model I, Fig. 3a) than for the partially blocked cavities (model II, Fig. 3c), whereas the mainstream normal flow showed opposite patterns (Fig. 3b and d). The present observations highlighted some effects of cavity blockage on the mean flow, consistent with those shown by previous studies (e.g. Gonzalez & Chanson, 2008; Takahashi et al., 2006;). Downstream of each step edge, a strong shear zone developed and expanded into the step cavity. The finding was consistent with previous

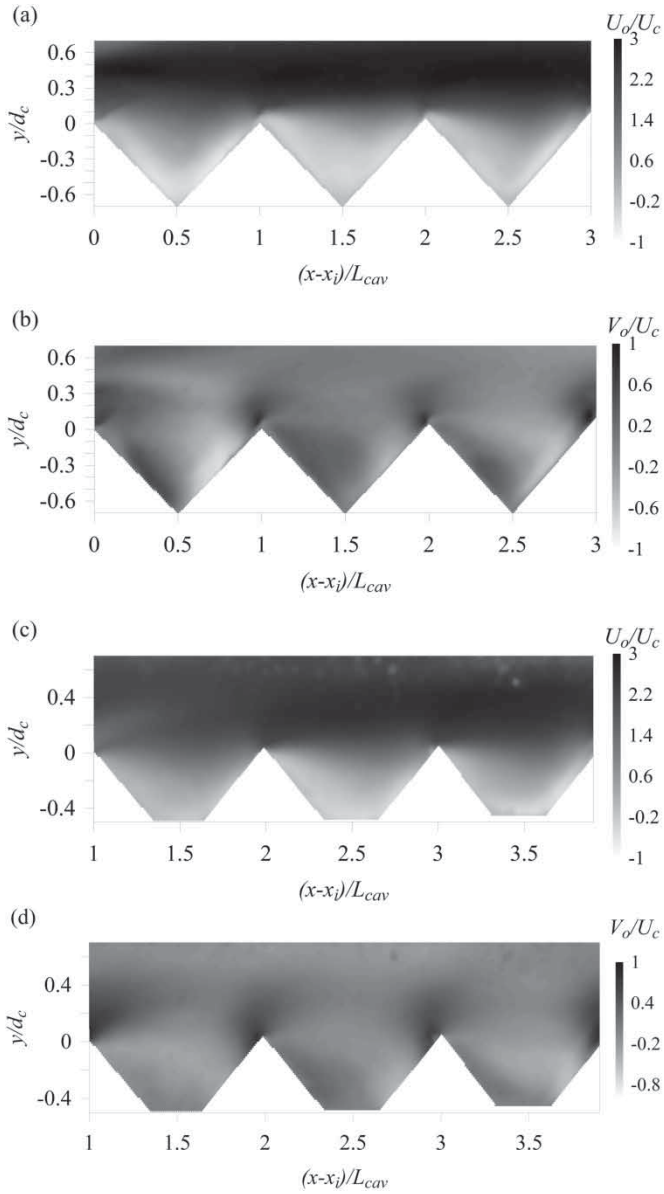


Figure 3 Mean streamwise and normal optical flow between step edges 5 and 8 in stepped chutes with triangular and modified step cavities: (a) streamwise optical flow in model I, (b) normal optical flow in model I, (c) streamwise optical flow in model II, (d) normal optical flow in model II. Flow conditions:  $d_c/h = 0.9$ ,  $h = 0.1$  m,  $\theta = 45^\circ$ . Flow direction from left to right

visual studies with BIV, PIV and optical flow (Amador et al., 2006; Bung, 2001; Bung & Valero, 2016a), and physical studies including Felder and Chanson (2011).

### 4.3 Mean flow deformations

The in-plane rate-of-strain ( $\epsilon_{o,xy}$ ) and spanwise vorticity ( $\omega_{o,z}$ ) distributions were calculated between step edges 5 and 8 in stepped chute models I and II (Fig. 4). These were obtained by taking derivatives of the mean optical flow field:

$$\epsilon_{o,xy} = \frac{\partial U_o}{\partial y} + \frac{\partial V_o}{\partial x} \quad (4)$$

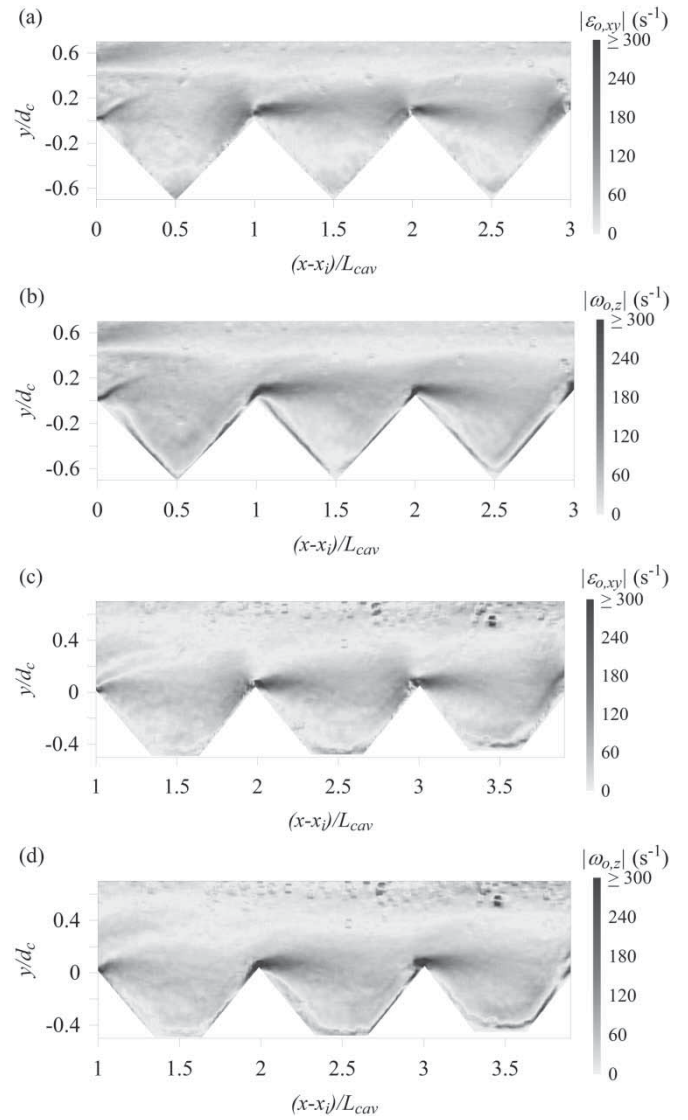


Figure 4 Optical mean flow deformations between step edges 5 and 8 in stepped chutes with triangular and modified step cavities: (a) shear rate vorticity in model I, (b) spanwise vorticity in model I, (c) shear rate in model II, (d) spanwise vorticity in model II. Flow conditions:  $d_c/h = 0.9$ ,  $h = 0.1$  m,  $\theta = 45^\circ$

$$\omega_{o,z} = \frac{\partial V_o}{\partial x} - \frac{\partial U_o}{\partial y} \quad (5)$$

where the derivatives were computed by convolving the mean optical flow with the respective Sobel filters of size  $3 \times 3$ :

$$\frac{\partial \mathbf{V}_o}{\partial x} = \frac{1}{8} \begin{bmatrix} -1 & 0 & 1 \\ -2 & 0 & 2 \\ -1 & 0 & 1 \end{bmatrix} * \mathbf{V}_o \quad (6)$$

$$\frac{\partial \mathbf{U}_o}{\partial y} = \frac{1}{8} \begin{bmatrix} 1 & 2 & 1 \\ 0 & 0 & 0 \\ -1 & 2 & -1 \end{bmatrix} * \mathbf{U}_o \quad (7)$$

where \* denotes convolution, and  $\mathbf{U}_o$  and  $\mathbf{V}_o$  are the streamwise and wall-normal optical flow fields, respectively.

For both triangular and partially blocked step cavities, the step edges were identified as the most significant source of turbulent production. The strain rate and vorticity were the largest in the immediate vicinity of the step edge, with magnitudes exceeding  $300 \text{ s}^{-1}$  (Fig. 4). This concentration of vorticity reflects relatively high velocity correlations and is dominantly small-scale, which may be responsible for high frequency instabilities in the shear layer (Lin & Rockwell, 2001). In addition, vorticities of significant magnitudes were observed to extend upstream along the bottom wall. The results were qualitatively and quantitatively consistent with those observed by Amador et al. (2006).

4.4 Turbulence intensity and turbulent kinetic energy fields

To characterize the apparent flow fluctuations, an optical turbulence intensity was defined as:

$$Tu_o = \sqrt{\overline{u'_o{}^2}}/U_o \tag{8}$$

where  $u'_o$  and  $U_o$  are the fluctuating and mean streamwise optical flows, respectively. Note that  $u'_o$  characterizes a combination of optical velocity fluctuations and noise caused by brightness variations. Figure 5 presents the optical turbulence intensity distributions for the present flow conditions in models I and II. In both models,  $Tu_o$  was mostly of the order of 0.1 in the mainstream, and a gradual increase in  $Tu_o$  was observed for decreasing elevation  $y$ . At the pseudo-bottom,  $Tu_o$  generally ranged between 0.3 and 0.6, except locally around the step edges where values over 100% were observed. These results were close to clear water data reported by Ohtsu and Yasuda (1997) and Amador et al. (2006). In most parts of the cavities,

extreme values of  $Tu_o$  in excess of 100% were recorded primarily on account of the slow fluid velocity. A detailed examination revealed slightly larger  $Tu_o$  values associated with the partial cavity blockage. Overall, the present data were much larger than those in smooth open channel flows (Nezu, 2005; Nezu & Nakagawa, 1993) and were generally in agreement with those reported by Bung and Valero (2016c).

The apparent turbulent motions can be further characterized by defining an optical turbulent kinetic energy ( $k_o$ ) in terms of the fluctuating optical flow components:

$$k_o = \frac{3}{4}(\overline{u'_o{}^2} + \overline{v'_o{}^2}) \tag{9}$$

where  $v'_o$  is the fluctuating normal optical flow. The present definition follows that adopted by Amador et al. (2006). The  $k_o$  distributions between step edges 5 and 8 were calculated for both models and are presented in Fig. 6. For both stepped chutes, the largest  $k_o$  values were identified near the pseudo-bottom, corresponding to significant shear layer velocity fluctuations sustained by removal of energy from the mean flow. Within the step cavities, the  $k_o$  values were generally negligible. This suggested that cavity recirculation alone might contribute little to the overall energy dissipation in skimming flows above stepped chutes. A comparison between models I and II indicated a general increase in  $k_o$  associated with the partial cavity blockage, which might be in part attributed to a reduction in the mutual sheltering between adjacent step elements. For both models, the dominant  $k_o$  values ranged between  $0.2$  and  $0.4 \text{ m}^2 \text{ s}^{-2}$ , which were consistent with the clear water PIV data of Amador et al. (2006).

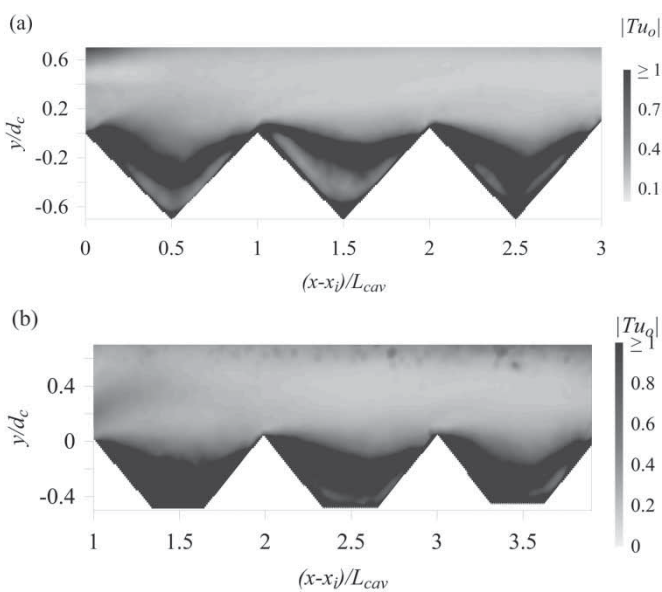


Figure 5 Streamwise optical turbulence intensity distributions between step edges 5 and 8 in stepped chutes with triangular and modified step cavities: (a) turbulence intensity in model I, (b) turbulence intensity in model II. Flow conditions:  $d_c/h = 0.9$ ,  $h = 0.1 \text{ m}$ ,  $\theta = 45^\circ$

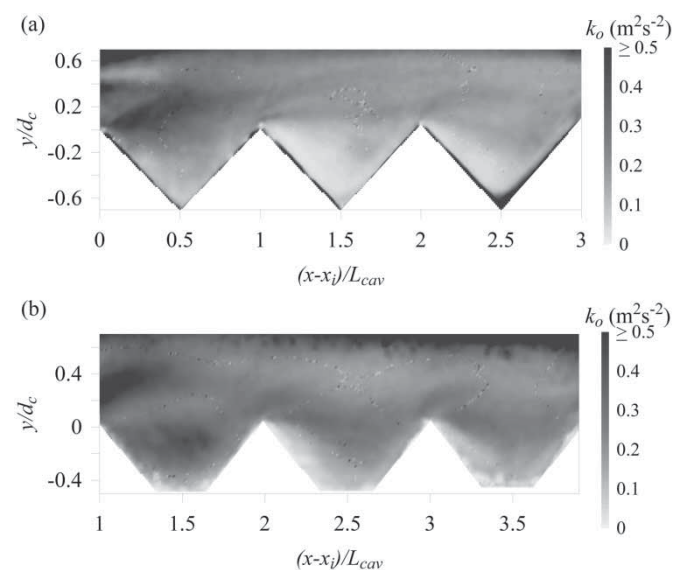


Figure 6 Optical turbulent kinetic energy distributions between step edges 5 and 8 in stepped chutes with triangular and modified step cavities: (a) turbulent kinetic energy in model I, (b) turbulent kinetic energy in model II. Flow conditions:  $d_c/h = 0.9$ ,  $h = 0.1 \text{ m}$ ,  $\theta = 45^\circ$

4.5 Scales of apparent turbulence

The largest apparent turbulent motions in the high-speed video data may be investigated by defining the relevant integral scales:

$$T_{x,o}(x_{im}, y_{im}) = \frac{1}{Tu_o'^2} \int_0^{\tau_0} \int_0^T u_o'(x_{im}, y_{im}, t) \times u_o'(x_{im}, y_{im}, t + \tau) dt d\tau \quad (10)$$

$$L_{x,o}(x_{im}, y_{im}) = \frac{1}{Tu_o'^2} \int_0^{\delta_0} \int_0^T u_o'(x_{im}, y_{im}, t) \times u_o'(x_{im} + \delta, y_{im}, t) dt d\delta \quad (11)$$

where  $T_{x,o}$  and  $L_{x,o}$  respectively characterize the time and length scales of the longest apparent connections observed from the video data,  $T$  is the total length of a video, and  $\tau_0$  and  $\delta_0$  are respectively the characteristic time lag and streamwise separation corresponding to the first zero-crossings of their respective inner integrals. Note that the present 32-bit implementation imposed a maximum 2 GB limit on memory usage; hence the outer integrals in the above definitions were computed up to the first zero-crossing, or 100 steps, whichever occurred first. Namely, the integral scales in the present context were obtained from normalized velocity correlations truncated for  $\tau > 0.022$  s and  $\delta > 32\text{--}36$  mm.

For the present flow conditions, the apparent integral time scale ( $T_{x,o}$ ) distributions between step edges 5 and 8 were computed for models I and II and presented in Fig. 7. For both models, large time scales associated with recirculatory fluid motions were identified in the step cavities. On the other hand, significant differences between the two stepped models were

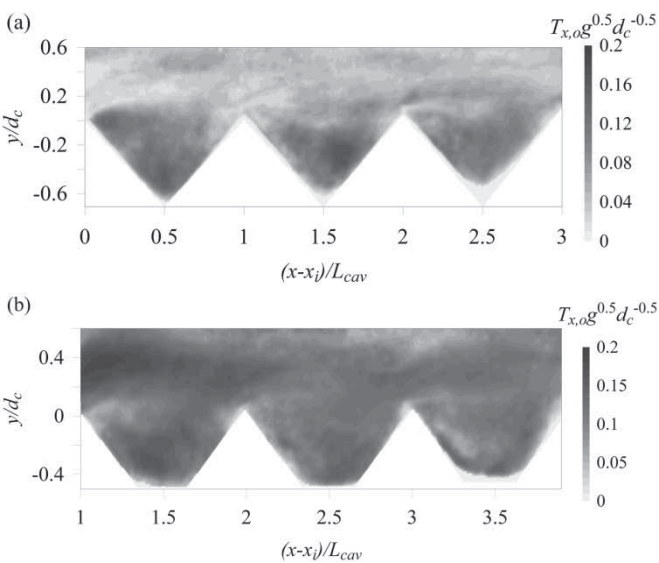


Figure 7 Optical integral time scale distributions between step edges 5 and 8 in stepped chutes with triangular and modified step cavities: (a) integral time scale in model I, (b) integral time scale in model II. Flow conditions:  $d_c/h = 0.9$ ,  $h = 0.1$  m,  $\theta = 45^\circ$

observed in the mainstream above the pseudo-bottom. The time scales in the mainstream above the triangular cavities were predominantly small, whereas those associated with the partially blocked cavities exhibited significant increases. The observation reflected differences in the vortex shedding dynamics linked to each cavity shape. Note that the present results are limited to one flow rate and might be subject to wall effects.

The corresponding integral length scales ( $L_{x,o}$ ) are presented in Fig. 8, where the data were non-dimensionalized in terms of the roughness height  $k$  (I:  $k = 7.1$  cm; II:  $k = 5.0$  cm). For both models, large-scale apparent coherent structures were identified within the step cavities. The mainstream flow in model II was associated with significantly larger scale apparent motion compared to model I. The mainstream large-scale structures exhibited sizes up to approximately  $0.5k$ , though underestimations were likely caused by truncated velocity correlations. Since  $T_{x,o}$  and  $L_{x,o}$  describe the large energy-containing structures, an apparent dissipation  $\epsilon_o$  may be defined such that  $T_{x,o} \sim k_o/\epsilon_o$  and  $L_{x,o} \sim k_o^{3/2}/\epsilon_o$ . The results would support the finding presented in Fig. 6, which showed substantially increased  $k_o$  induced by partial blockage to the step cavities.

The rapid turbulent fluctuations recorded by the video camera may be characterized by the relevant microscales deduced from velocity correlation functions at the origin:

$$\tau_{x,o} = \left( - \frac{\partial^2 R_{u_o}(t)}{\partial t^2} \Big|_{t=0} \right)^{(-1/2)} \quad (12)$$

$$\lambda_{x,o} = \left( - \frac{\partial^2 R_{u_o}(x)}{\partial x^2} \Big|_{x=0} \right)^{(-1/2)} \quad (13)$$

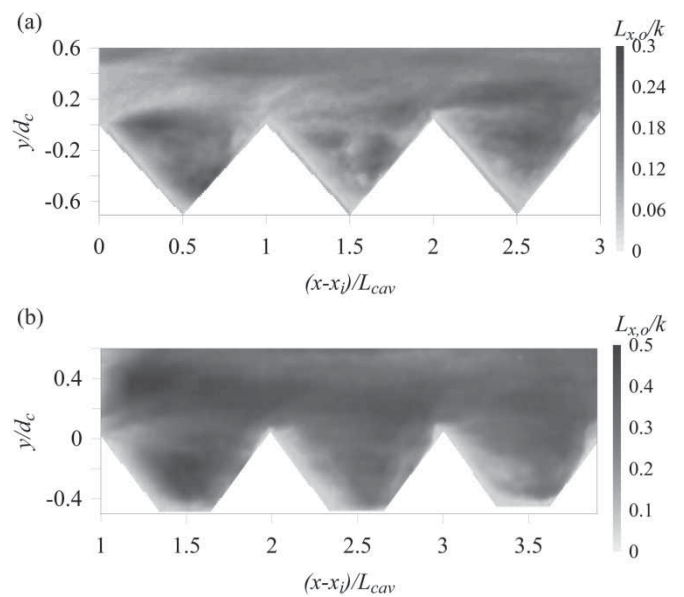


Figure 8 Optical integral length scale distributions between step edges 5 and 8 in stepped chutes with triangular and modified step cavities: (a) integral length scale in model I, (b) integral length scale in model II. Flow conditions:  $d_c/h = 0.9$ ,  $h = 0.1$  m,  $\theta = 45^\circ$

where  $R_{u_o}$  is the normalized correlation function calculated from  $u_o$  as either a function of space or time. The second derivatives were obtained by convolving the respective correlation functions with a finite difference filter and assuming that  $R_{u_o}$  is symmetrical:

$$\left. \frac{\partial^2 R_{u_o}(x)}{\partial x^2} \right|_{x=0} = \frac{1}{6}(-15R_{u_o}(0) + 16R_{u_o}(1) - R_{u_o}(2)) \quad (14)$$

In addition, the microscales  $\lambda_{x,o}$  is related to the fluctuating optical flow derivative by:

$$\lambda_{x,o}^2 \sim \left( \left( \frac{\partial u'_o}{\partial x} \right)^2 \right)^{-1} \quad (15)$$

Likewise, one can show that  $\tau_{x,o}^2 \sim \overline{((\partial u'_o/\partial x)^2)}^{-1}$  by invoking Taylor's hypothesis (where  $Tu_o \ll 1$ ). Note that in homogeneous isotropic turbulence the dissipation  $\epsilon$  is proportional to the streamwise turbulent velocity derivative  $(\partial u'/\partial x)^2$  (Pope, 2000).

The distributions of micro time scale  $\tau_{x,o}$  were calculated between step edges 5 and 8 and are presented for both models in Fig. 9. Typically,  $\tau_{x,o}$  were approximately 1–2 orders of magnitude smaller than the integral time scale  $T_{x,o}$ , and corresponded to 0.002–0.008 s physically. This implied a minimum sampling rate of approximately 1000 Hz required to capture adequately the small-scale fluctuations influenced by viscosity directly. A further inspection showed generally larger  $\tau_{x,o}$  values in model II, which implied some changes in fluctuating velocity derivatives caused by the partial cavity blockage.

The corresponding distributions of  $\lambda_{x,o}$  for both models are presented in Fig. 10. Typical values of  $\lambda_{x,o}$  ranged between

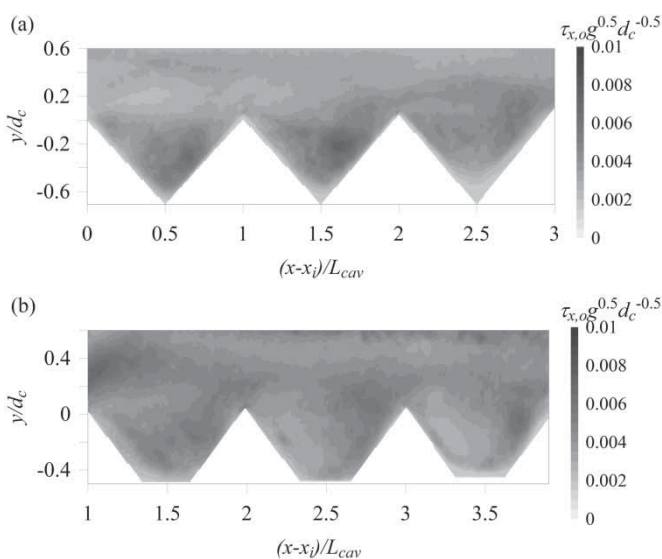


Figure 9 Optical micro time scale distributions between step edges 5 and 8 in stepped chutes with triangular and modified step cavities: (a) micro time scale in model I, (b) micro time scale in model II. Flow conditions:  $d_c/h = 0.9$ ,  $h = 0.1$  m,  $\theta = 45^\circ$

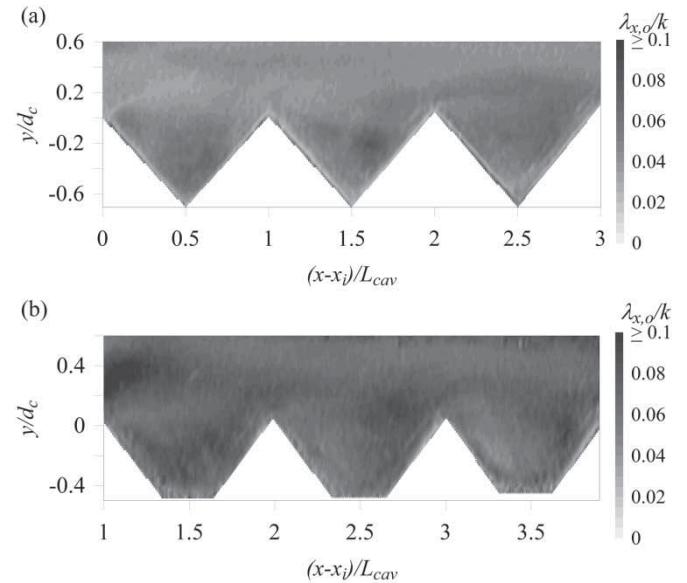


Figure 10 Optical micro length scale distributions between step edges 5 and 8 in stepped chutes with triangular and modified step cavities: (a) micro length scale in model I, (b) micro length scale in model II. Flow conditions:  $d_c/h = 0.9$ ,  $h = 0.1$  m,  $\theta = 45^\circ$

0.01 $k$  and 0.1 $k$ , substantially smaller than the integral scale  $L_{x,o}$ . The findings imposed a minimum resolution constraint of approximately 0.5 mm px<sup>-1</sup> on the high-speed videos; hence the physical resolutions of the present videos were deemed to be appropriate. The present data revealed a significant increase in  $\lambda_{x,o}$  associated with the partial cavity blockage, which corroborated with Fig. 9. Note that the data accuracy might be affected by the assumption of symmetry in  $R_{u_o}$  near the origin.

Overall, the present data suggested that partial step cavity blockage might be associated with some increase in micro-time and length scales, hence a decrease in the velocity gradient fluctuation  $(\partial u'_o/\partial x)^2$ . This likely reflected a change in the dissipation  $\epsilon$ , and consequently a modification of the turbulent kinetic energy budget. Importantly, the cavity shape was shown to play a pivotal role in determining the turbulent characteristics of aerated skimming flows.

### 5 Conclusion

The effects of cavity shape on a high-speed aerated skimming flow were investigated non-intrusively using a local optical flow approach. Detailed video investigations were performed with an ultra-high-speed camera recording at 22,607 fps (subsampling at 4521 fps) in a large-size stepped spillway model configured with triangular and trapezoidal cavities. The results highlighted significant impacts of partial cavity blockage on the mean and turbulence properties of an aerated skimming stepped chute flow.

The mean flow fields for both triangular and trapezoidal cavities appeared qualitatively similar, consisting of a skimming

mainstream and a recirculating cavity region. Relative to the triangular cavities, the trapezoidal cavities displayed a decrease in streamwise flow above the pseudo-bottom. The rate-of-strain and vorticity fields highlighted the step edge as the most significant source of turbulent production, and the cavity shape appeared to have little influence. For both models, the streamwise turbulence intensity was small in the mainstream, and gradually increased to 30–60% next to the pseudo-bottom. Significant turbulent kinetic energy levels were associated with the shear layer development trailing each step edge. The trapezoidal cavities appeared to be associated with elevated turbulence levels compared to the triangular cavities. The findings were in agreement with previous clear water LDA and PIV data and highlighted the turbulent nature of stepped chute flows in contrast to typical smooth open channel flows.

The apparent turbulent motion was characterized by computing the relevant integral and micro time and length scales. The results highlighted increased large-scale motions in the mainstream flow above trapezoidal cavities, possibly linked to a reduction in mutual sheltering between adjacent step elements. The partial cavity blockage resulted in increased micro time and length scales, thus reflecting a reduction in the associated velocity derivative fluctuations. The microscales imposed constraints on the minimum sampling requirements, which were satisfied in the present study.

Overall, the present optical flow study emphasized the extremely turbulent and complex nature of aerated stepped chute flows. The findings showed modifications of the air–water flow properties resulting from different cavity shapes. They offered new insights into the near wall turbulent flow structures. It is believed that the non-intrusive approach adopted herein should be applied to complement existing metrologies in other types of air–water flows.

### Acknowledgements

The authors thank Professor Daniel Bung (FH Aachen, Germany) for his detailed review of and valuable comments on the original report on which this paper is based. The authors acknowledge the technical assistance of Jason Van Der Gevel and Steward Matthews (University of Queensland, Australia). The first author was the recipient of an Australian Postgraduate Award during his Ph.D.

### Funding

This work was supported by the Australian Research Council [grant number DP120100481].

### Notation

$d$  = displacement vector (m)  
 $d_c$  = critical depth (m)

$g$  = gravitational acceleration ( $\text{m s}^{-2}$ )  
 $h$  = step height (m)  
 $H_1$  = upstream head above crest (m)  
 $I$  = image intensity (–)  
 $k$  = roughness height (m)  
 $k_o$  = optical turbulent kinetic energy ( $\text{m}^2 \text{s}^{-2}$ )  
 $l$  = step length (m)  
 $L_{cav}$  = cavity length (m)  
 $L_{crest}$  = length of upstream broad-crested weir (m)  
 $L_{x,o}$  = optical autocorrelation length scale (m)  
 $Q$  = discharge ( $\text{m}^3 \text{s}^{-1}$ )  
 $R_{uo}$  = normalized correlation coefficient calculated from  $u_o$  (–)  
 $t$  = time (s)  
 $T$  = total video duration (s)  
 $T_{x,o}$  = optical autocorrelation time scale (s)  
 $Tu_o$  = optical turbulence intensity (–)  
 $u_o$  = optical flow vector ( $= (u_o, v_o)^T$ ) ( $\text{m s}^{-1}$ )  
 $u_o$  = instantaneous streamwise optical flow ( $\text{m s}^{-1}$ )  
 $u_o'$  = streamwise optical flow fluctuation ( $\text{m s}^{-1}$ )  
 $U_c$  = critical velocity ( $\text{m s}^{-1}$ )  
 $U_o$  = mean streamwise optical flow ( $\text{m s}^{-1}$ )  
 $v_o$  = instantaneous normal optical flow ( $\text{m s}^{-1}$ )  
 $v_o'$  = normal optical flow fluctuation ( $\text{m s}^{-1}$ )  
 $V_o$  = mean normal optical flow ( $\text{m s}^{-1}$ )  
 $W$  = channel width (m)  
 $x$  = streamwise coordinate (m)  
 $x_i$  = streamwise position of inception point (m)  
 $x_{im}$  = horizontal image coordinate (m)  
 $y$  = normal coordinate (m)  
 $y_{im}$  = vertical image coordinate (m)  
 $\epsilon_o$  = apparent dissipation ( $\text{m}^2 \text{s}^{-3}$ )  
 $\epsilon_{o,xy}$  = in-plane rate-of-strain ( $\text{s}^{-1}$ )  
 $\delta$  = streamwise offset (m)  
 $\delta_0$  = streamwise offset at which an autocorrelation function first crosses zero (m)  
 $\theta$  = chute slope ( $^\circ$ )  
 $\lambda_{x,o}$  = optical Taylor micro-length scale (m)  
 $\tau$  = time lag (s)  
 $\tau_{x,o}$  = optical Taylor micro-time scale (s)  
 $\tau_0$  = time lag at which an autocorrelation function first crosses zero (s)  
 $\omega$  = spanwise vorticity ( $\text{s}^{-1}$ )

### ORCID

Gangfu Zhang  <http://orcid.org/0000-0002-3368-7326>  
 Hubert Chanson  <http://orcid.org/0000-0002-2016-9650>

### References

Adelson, E., Anderson, C. H., Bergen, J. R., Burt, P. J., & Ogden, J. M. (1984). Pyramid methods in image processing. *RCA Engineer*, 29(6), 33–41.



- Amador, A., Sánchez-Juny, M., & Dolz, J. (2006). Characterization of the nonaerated flow region in a stepped spillway by PIV. *Journal of Fluids Engineering*, 128(6), 1266–1273. doi:10.1115/1.2354529
- Bung, D. B. (2011, 26 June–1 July). Non-intrusive measuring of air–water flow properties in self-aerated stepped spillway flow. In Eric Valentine, Colin Apelt, James Ball, Hubert Chanson, Ron Cox, Rob Ettema, George Kuczera, Martin Lambert, Bruce Melville, & Jane Sargison (Eds.), *Proceedings of 34th IAHR World Congress* (pp. 2380–2387). Brisbane, Australia: Engineers Australia Publication.
- Bung, D. B., & Valero, D. (2016a). Optical flow estimation in aerated flows. *Journal of Hydraulic Research*, 54(5), 1–6.
- Bung, D. B., & Valero, D. (2016b, 27–30 June). Application of the optical flow method to velocity determination in hydraulic structure models. In B. Crookston, & B. Tullis (Eds.), *Proceedings of 6th IAHR International Symposium on Hydraulic Structures* (pp. 50–60). Portland OR: Hydraulic Structures and Water System Management.
- Bung, D. B., & Valero, D. (2016c, 27–29 July). Image processing techniques for velocity estimation in highly aerated flows: bubble image velocimetry vs. optical flow. *Proc. 4th IAHR Europe Congress* (pp. 151–157). Liege, Belgium.
- Bung, D. B., & Valero, D. (2017). FlowCV – An open-source toolbox for computer vision applications in turbulent flows. In Aminuddin Ab. Ghani, Ngai Weng Chan, Junaidah Ariffin, Ahmad Khairi Abd Wahab, Sobri Harun, Amir Hashim Mohamad Kassim, & Othman Karim (Eds.), *Proceedings of 37th IAHR World Congress*. Kuala Lumpur, Malaysia: USAINS Holding Sdn. Bhd. Publ.
- Burt, P. J., & Adelson, E. H. (1983). The Laplacian pyramid as a compact image code. *IEEE Transactions on Communications*, 31(4), 532–540.
- Chanson, H. (1993). Stepped spillway flows and air entrainment. *Canadian Journal of Civil Engineering*, 20(3), 422–435. doi:10.1139/193-057.
- Chanson, H. (1994). Hydraulics of skimming flows over stepped channels and spillways. *Journal of Hydraulic Research*, 32(3), 445–460. doi:10.1080/00221689409498745
- Chanson, H. (2001). *The hydraulics of stepped chutes and spillways*. Lisse, The Netherlands: Balkema.
- Chanson, H. (2008). Advective diffusion of air bubbles in turbulent water flows. In C. Gualtieri & D.T. Mihailovic (Eds.), *Fluid mechanics of environmental interfaces* (pp. 163–196). Leiden, The Netherlands: Taylor & Francis.
- Chanson, H., Yasuda, Y., & Ohtsu, I. (2002). Flow resistance in skimming flows in stepped spillways and its modelling. *Canadian Journal of Civil Engineering*, 29(6), 809–819. doi:10.1139/102-083.
- Chen, J., & Katz, J. (2005). Elimination of peak locking error in PIV analysis using the correlation mapping method. *Measurement Science and Technology*, 16(8), 1605.
- Corpetti, T., Heitz, D., Arroyo, G., Memin, E., & Santa Cruz, A. (2006). Fluid experimental flow estimation based on an optical flow scheme. *Experiments in Fluids*, 40(1), 80–97.
- Djenidi, L., Elavasaran, R., & Antonia, R. A. (1999). The turbulent boundary layer over transverse square cavities. *Journal of Fluid Mechanics*, 395, 271–294.
- Ervine, D. A., & Falvey, H. T. (1987). Behaviour of turbulent water jets in the atmosphere and in plunge pools. *Proceedings of the Institution of Civil Engineers*, 83, 295–314.
- Farneback, G. (2003). Two-frame motion estimation based on polynomial expansion. *Image Analysis, Springer Berlin Heidelberg*, 363–370.
- Felder, S., & Chanson, H. (2011). Air-water flow properties in step cavity down a stepped chute. *International Journal of Multiphase Flow*, 37(7), 732–745. doi:10.1016/j.ijmultiphaseflow.2011.02.009
- Gonzalez, C. A., & Chanson, H. (2004). Interactions between cavity flow and main stream skimming flows: An experimental study. *Canadian Journal of Civil Engineering*, 31(1), 33–44.
- Gonzalez, C. A., & Chanson, H. (2008). Turbulence manipulation in air–water flows on a stepped chute: An experimental study. *European Journal of Mechanics - B/Fluids*, 27(4), 388–408. doi:10.1016/j.euromechflu.2007.09.003
- Guenther, P., Felder, S., & Chanson, H. (2013). Flow aeration, cavity processes and energy dissipation on flat and pooled stepped spillways for embankments. *Environmental Fluid Mechanics*, 13(5), 503–525. doi:10.1007/s10652-013-9277-4
- Horn, B. K., & Schunck, B.G. (1981). Determining optical flow. *Artificial Intelligence*, 17(1-3), 185–203.
- Leandro, J., Bung, D. B., & Carvalho, R. (2014). Measuring void fraction and velocity fields of a stepped spillway for skimming flow using non-intrusive methods. *Experiments in Fluids*, 55(5), 1732.
- Lin, J. C., & Rockwell, D. (2001). Organised oscillations of initially turbulent flow past a cavity. *AIAA Journal*, 39(8), 1139–1151.
- Liu, T., Merat, A., Makhmalbaf, M. H. M., Fajardo, C., & Merati, P. (2015). Comparison between optical flow and cross-correlation methods for extraction of velocity fields from particle images. *Experiments in Fluids*, 56(8), 1–23.
- Lucas, B. D., & Kanade, T. (1981). An iterative image registration technique with an application to stereo vision. *IJCAI*, 81(1), 674–679.
- Nezu, I. (2005). Open-channel flow turbulence and its research prospect in the 21st century. *Journal of Hydraulic Engineering*, 131(4), 229–246.
- Nezu, I., & Nakagawa, H. (1993). *Turbulence in open-channel flows*. IAHR Monograph, IAHR Fluid Mechanics Section. Rotterdam, The Netherlands: Balkema Publ.
- Ohtsu, I., & Yasuda, Y. (1997). Characteristics of flow conditions on stepped channels. In F. M. Holly Jr., & A. Alsaffar (Eds.), *Proc. 27th IAHR Congress* (pp. 583–588). Theme D, San Francisco, USA.

- Perry, A. E., Schofield, W. H., & Joubert, P. N. (1969). Rough wall turbulent boundary layers. *Journal of Fluid Mechanics*, 37, 383–413. doi:10.1017/s0022112069000619
- Pope, S. B. (2000). *Turbulent flows*. Cambridge, New York, NY: Cambridge University Press.
- Rao, N. S. G., & Rajaratnam, N. (1961). On the inception of air entrainment in open channel flows. *Proceedings of 9th IAHR Biennial Congress* (pp. 9–12). Dubrovnik, Yugoslavia.
- Takahashi, M., Gonzalez, C. A., & Chanson, H. (2006). Self-aeration and turbulence in a stepped channel: Influence of cavity surface roughness. *International Journal of Multiphase Flow*, 32, 1370–1385. doi:10.1016/j.ijmultiphaseflow.2006.07.001
- Wood, I. R., Ackers, P., & Loveless, J. (1983). General method for critical point on spillways. *Journal of Hydraulic Engineering*, 109, 308–312. doi:10.1061/(asce)0733-9429(1983)109:2(308)
- Zhang, G., & Chanson, H. (2016a). Gabion stepped spillway: Interactions between free-surface, cavity, and seepage flows. *Journal of Hydraulic Engineering*, 142(5), 5. Paper 06016002. doi:10.1061/(ASCE)HY.1943-7900.0001120.
- Zhang, G., & Chanson, H. (2016b). Hydraulics of the developing flow region of stepped spillways. I: physical modelling and boundary layer development. *Journal of Hydraulic Engineering*, 142(7), 8. doi:10.1061/(ASCE)HY.1943-7900.0001138
- Zhang, G., & Chanson, H. (2018). Application of local optical flow methods to high-velocity free-surface flows: Validation and application to stepped chutes. *Experimental Thermal and Fluid Science*, 90, 186–199.